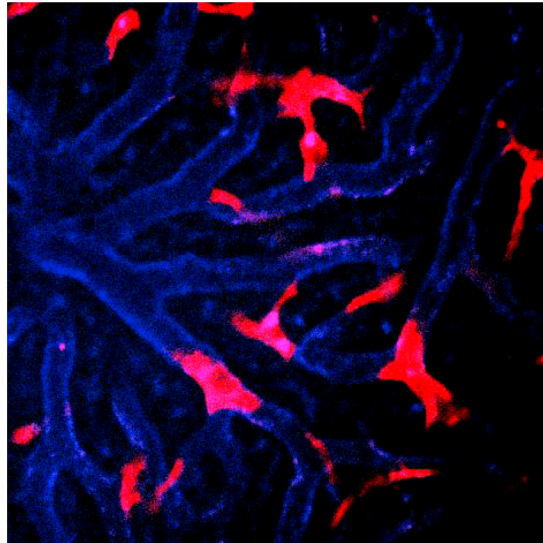


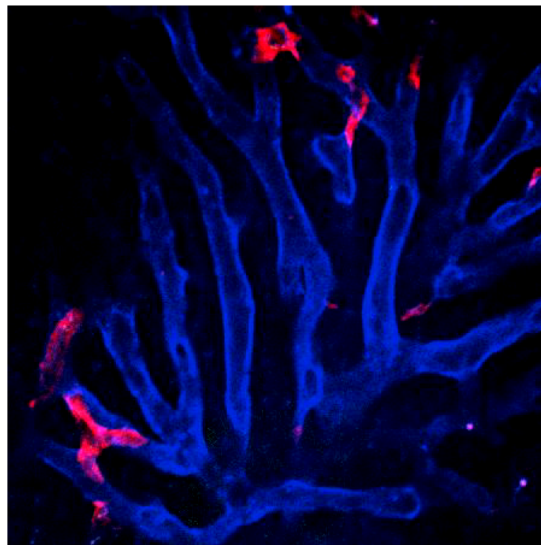
**Supplemental Figure 1. Coating of fluorescent microspheres with VWF.**

100 nm fluorescent polystyrene microspheres were coated with VWF, glycine, and BSA according to manufacturer's protocols. (A) Murine stabilin-2 expressing and control cells were exposed to coated microspheres. Uncoated microspheres bound to stabilin-2 expressing and control cells. VWF and BSA-coated microspheres (positive control) bound to stabilin-2 expressing cells only. Glycine-coated microspheres (negative control) did not bind to stabilin-2-expressing or control cells. (B) Confirmation of VWF coating was demonstrated by binding to anti-VWF antibody using a solid phase assay.

A. Uncoated microspheres

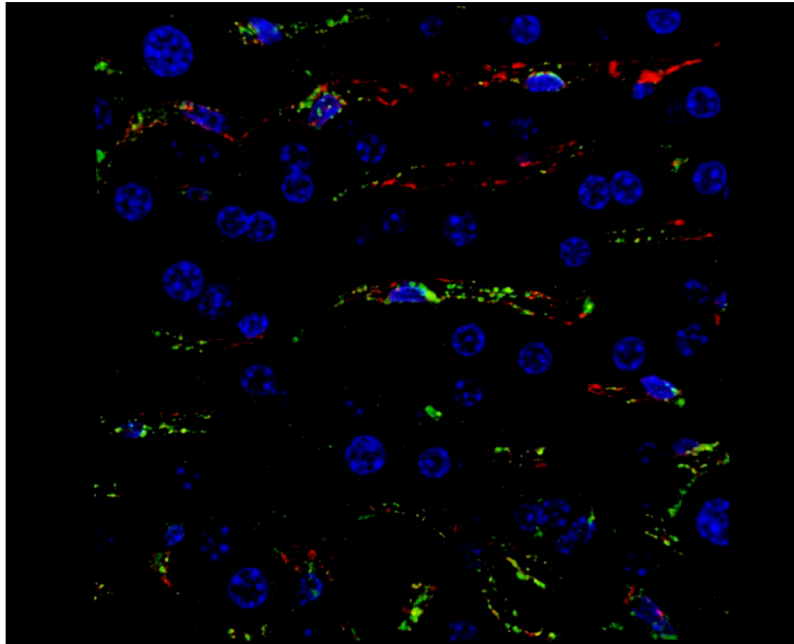


B. VWF-coated microspheres

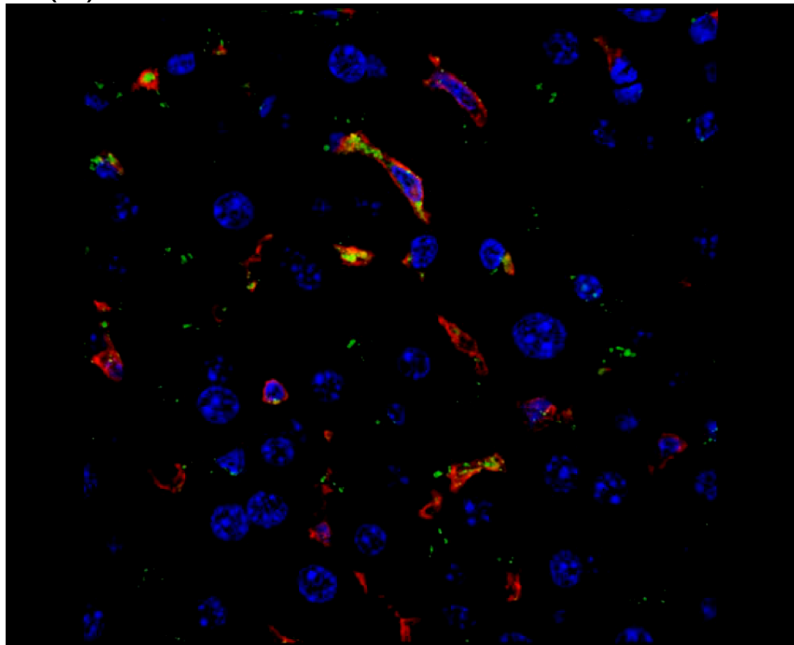


**Supplemental Figure 2. Intravital imaging of association of VWF-coated microspheres with LSECs and KCs.** (A) Uncoated microspheres, and (B) VWF-coated microspheres. Time lapse over 3 minutes. LSECS (CD31) = blue, Kupffer cells (F4/80) = red, fluorescent microspheres = green/yellow.

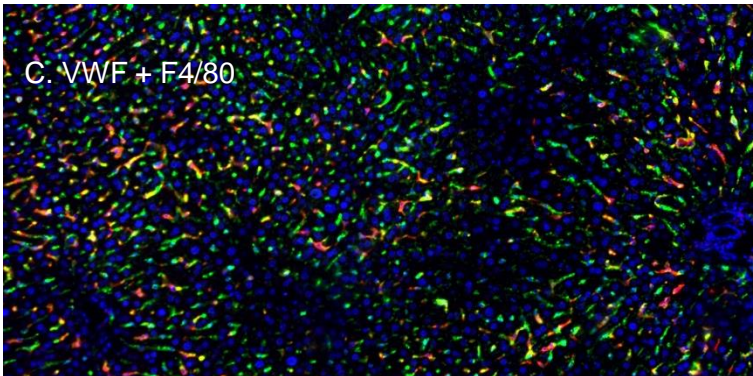
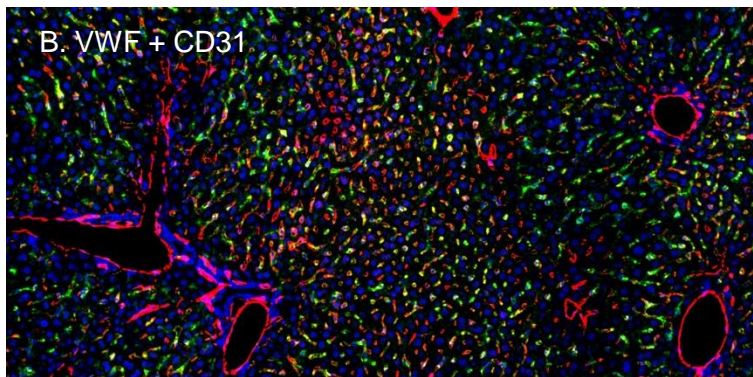
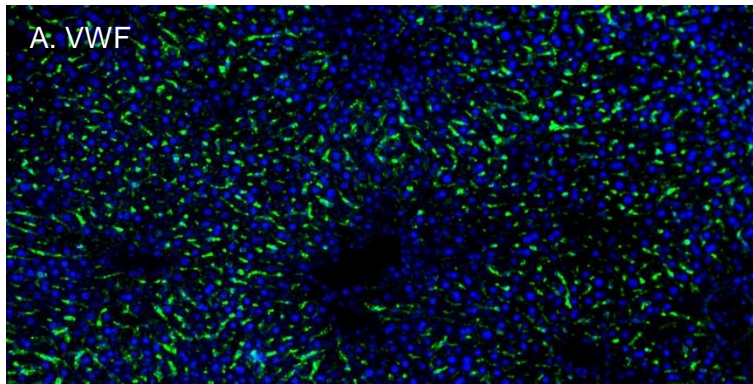
(A) VWF and LSECs



(B) VWF and KCs

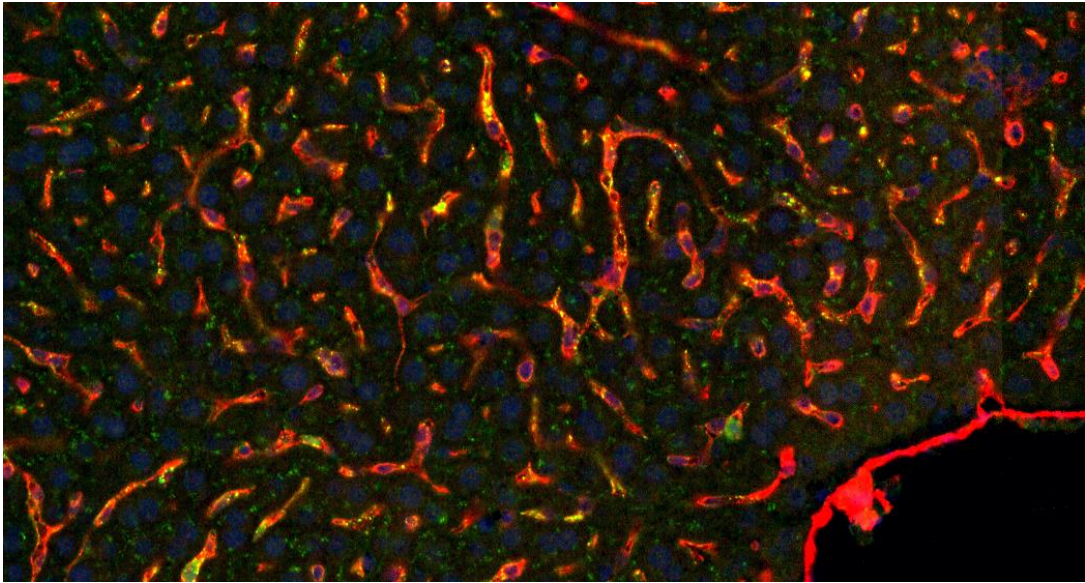


**Supplemental Figure 3. 3-dimensional image reconstruction of VWF association with LSECs and KCs in the murine liver.** VWF KO mice were infused with 200 mg/kg human pdVWF. 30 minutes post-infusion livers were perfused and fixed in formalin, and paraffin-embedded. 7  $\mu$ m sections were stained for VWF, LSECs (anti-CD31), or KCs (anti-F4/80). Sections were imaged using two-photon confocal microscopy (SP8 Tandem Scanner, Leica), and 3-dimensional reconstruction was performed using Fiji. (A) Association of infused VWF (green) with LSECs (red). (B) Association of infused VWF (green) with Kupffer cells (red).

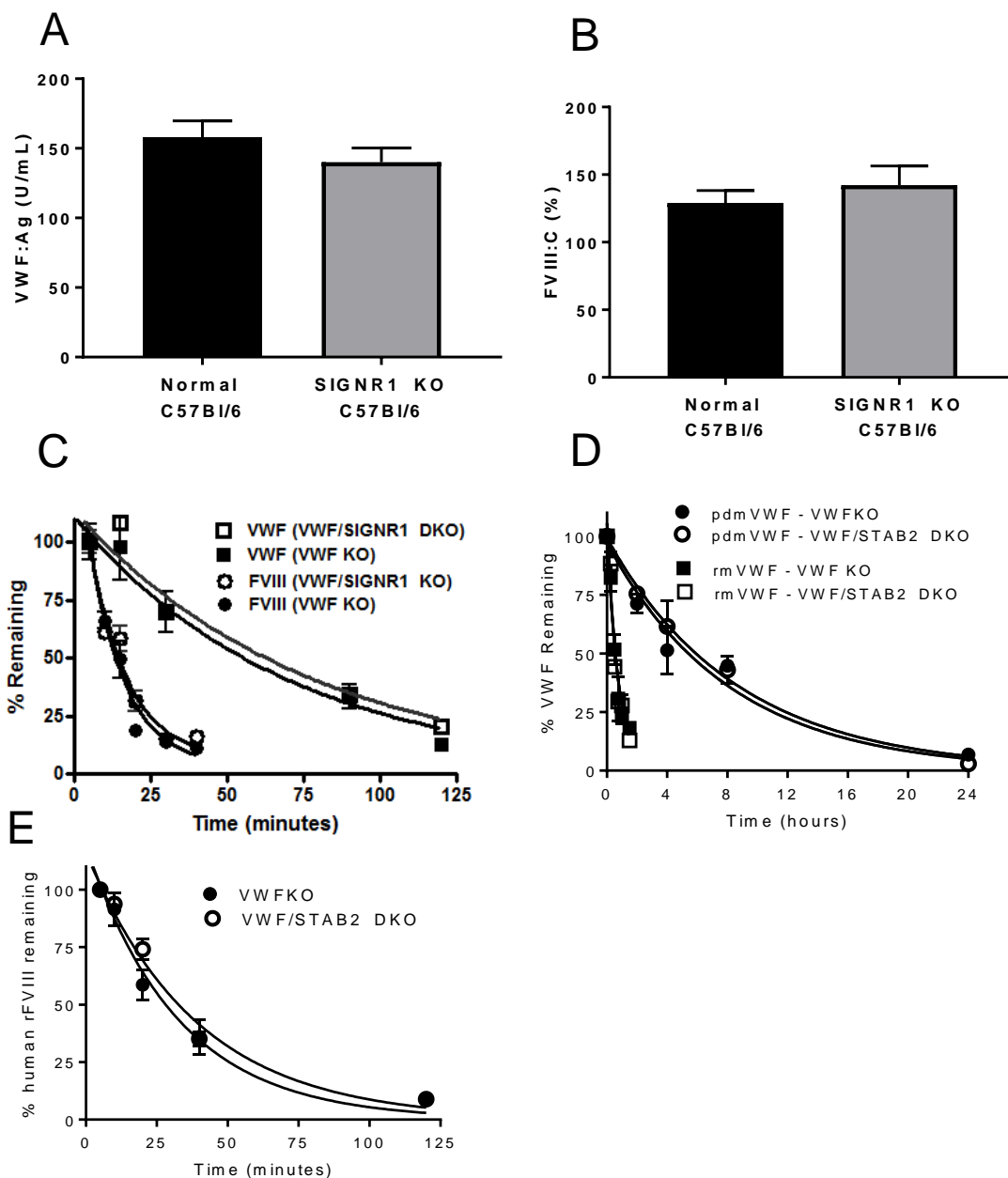


**Supplemental Figure 4. VWF is not evenly distributed throughout the liver.** VWF KO mice were infused with human pdVWF (200 U/kg) for 30 minutes. (A) Livers were stained for: VWF (green) and DAPI (blue). (B) VWF (green), CD31 (red), and DAPI (blue). (C) VWF (green), F4/80 (red), and DAPI (blue).





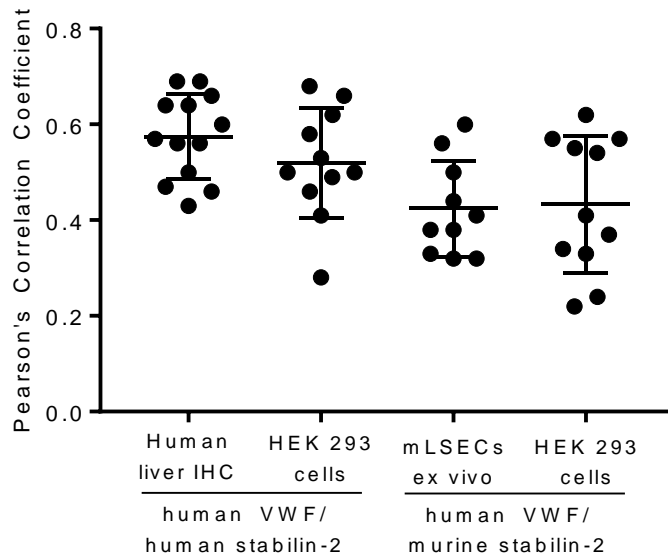
**Supplemental Figure 5. Murine VWF associates with CD31 positive and CD31 negative cells in the murine liver.** VWF KO mice were infused with murine VWF for 30 minutes. VWF (green) associates with CD31-positive (red) cells and CD31-negative cells.



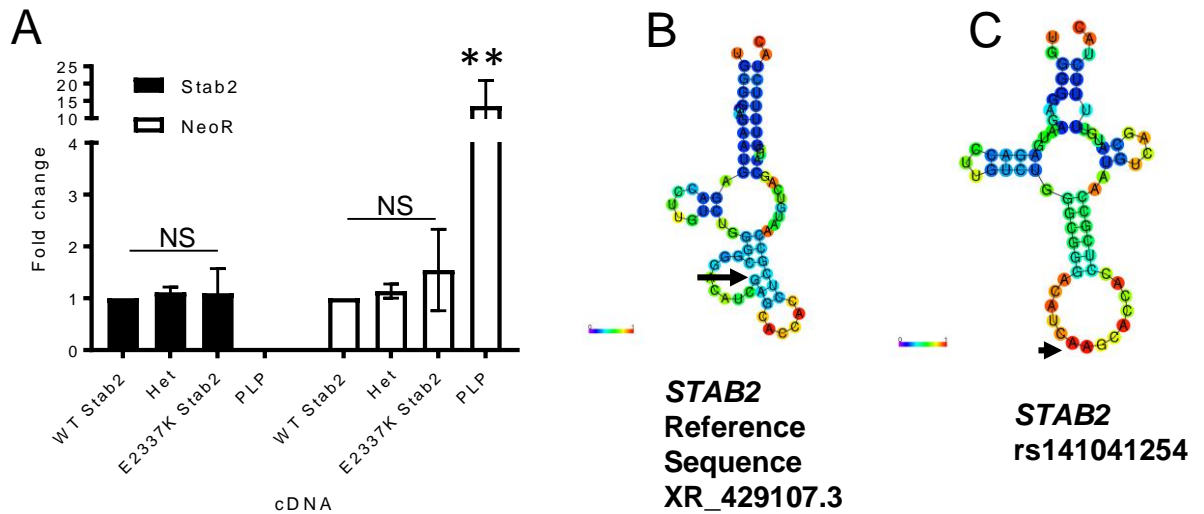
### Supplemental Figure 6. Clearance of VWF and FVIII by SIGNR1 and stabilin-2.

The influence of SIGNR1, a murine homologue of human CLEC4M on the clearance of VWF-FVIII was assessed in a SIGNR1 KO and VWF/SIGNR1 DKO mouse model. (A) SIGNR1 deficiency did not influence endogenous VWF:Ag levels compared with normal C57Bl/6 mice. (B) SIGNR1 deficiency did not influence endogenous FVIII:C compared with normal C57Bl/6 mice. (C) SIGNR1 deficiency did not influence the half-life of human pdVWF or rFVIII.

The clearance of murine VWF and human recombinant VWF was assessed in VWF/STAB2 DKO compared with VWF KO controls. (D) STAB2 deficiency did not influence the half life of murine recombinant or plasma-derived VWF. (E) STAB2 deficiency did not modify the half life of human recombinant FVIII in the absence of VWF.



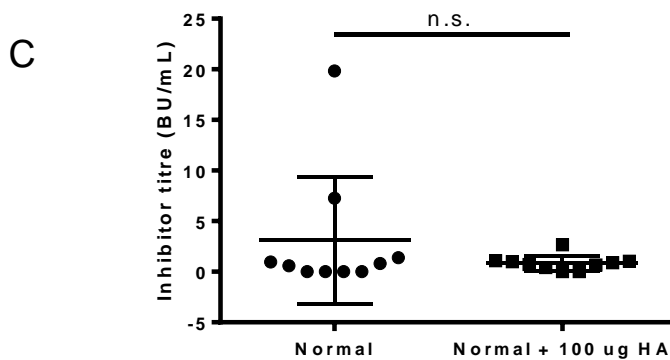
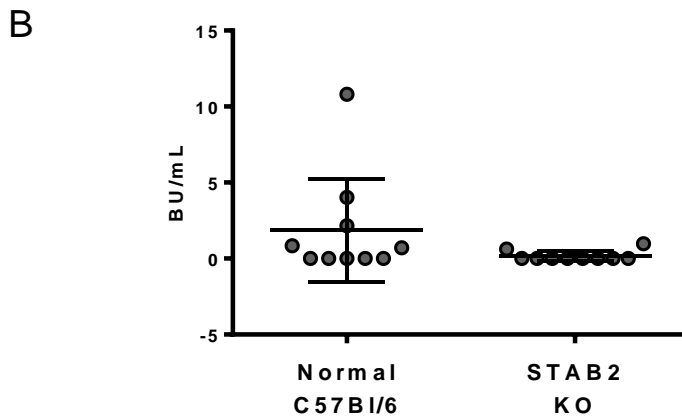
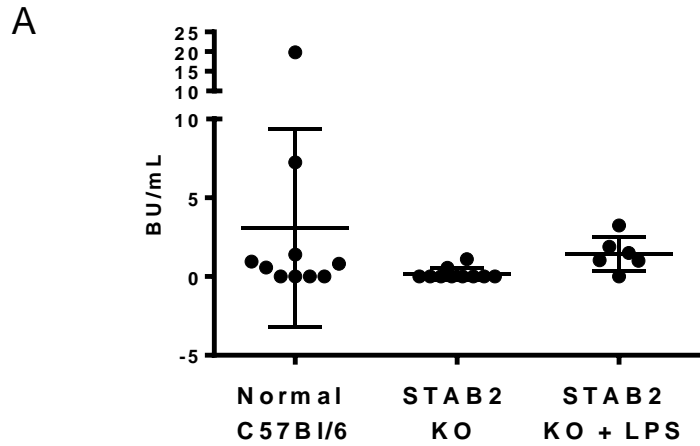
**Supplemental Figure 7.** To confirm that VWF co-localizes with stabilin-2, we performed image analysis using to quantify co-localization by Pearson's correlation coefficient using the Fiji Coloc2 plugin. We observed that for individual stabilin-2 expressing cells, the VWF antigen signal was positively associated with a stabilin-2 signal. As previous studies have demonstrated that once stabilin-2 has endocytosed its ligand, it is rapidly returned to the cell surface via recycling endosomes. Moreover, LSECs may express additional receptors that can contribute to the endocytosis of VWF by these cells. Therefore, a perfect positive correlation (+1) would not be expected.



**Supplemental Figure 8. The *STAB2* rs141041254 SNV alters *STAB2* mRNA levels and secondary structure.** To assess the influence of the *STAB2* SNV rs141041254 on *STAB2* mRNA production, we performed Taqman gene expression analysis on HEK 293 cells that were transiently transfected with equimolar wild-type *STAB2* cDNA and the *STAB2* E2377K variant. To control for number of transfected cells and transfection efficiency, endogenous *GAPDH* and *NEOR* (the resistance cassette expressed on the pLP vector) gene expression was quantified in parallel. Error bars  $\pm$  SD. \*\* $p \leq 0.0001$

Additionally we performed in silico analysis to determine the influence of the *STAB2* rs141041254 SNV on the mRNA secondary structure using CentroidFold ([rtools.cbrc.jp/centroidfold/](http://rtools.cbrc.jp/centroidfold/)) under default settings. CentroidFold predicts that the rs141041254 alters RNA secondary structure which has been linked with RNA stability and translation efficiency.





**Supplemental Figure 9. Influence of stabilin-2 deficiency and hyaluronic acid on FVIII inhibitors.**

Bethesda analysis of FVIII inhibitors was performed. (A) Mice treated IV with pdFVIII  $\pm$  LPS. (B) Mice treated IV with rFVIII. (C) Mice treated with pdFVIII  $\pm$  hyaluronic acid.



	Murine VWF	Human VWF	Human FVIII (VWF-free)	Human FVIII (+ mVWF)	Human FVIII (+ hVWF)
Binds LSECs	Yes	Yes	Low	N/A	Yes
Cleared by LSECs	Yes	Yes	N/A	Yes	N/A
Binds Stabilin-2	No	Yes	No	N/A	Yes
Cleared by Stabilin-2	No	Yes	No	N/A	Yes
Immune response by stabilin-2	N/A	Yes	N/A	Not significant	Yes

Supplemental Table 1. Summary of study observations involving murine versus human VWF  
N/A = not available